AIMS Materials Science, 4(2): 470-486.
DOI: 10.3934/matersci.2017.2.470
Received: 10 January 2017
Accepted: 14 March 2017
Published: 21 March 2017

http://www.aimspress.com/journal/Materials

Research article

Electrokinetic aspects of water filtration by AlOOH-coated siliceous particles with nanoscale roughness

Leonid A. Kaledin *, Fred Tepper, and Tatiana G. Kaledin

Chemistry Department, Argonide Corporation, 291 Power Court, Sanford, FL 32771, USA

*** Correspondence:** Email: kaledin@argonide.com; Tel: 407-322-2500; Fax: 407-322-1144.

Abstract: The vast majority of analytical and numerical models developed to explain pressure-driven electrokinetic phenomena assume that the local electrical double layer field over heterogenious surfaces is independent of the flow field and described by the Poison-Boltzman equation. However, for pressure-driven flow over a surface with heterogeneous patches with combined microscale and nanoscale structures the local electrical double layer fields are different above the patch and in the region between the patches. The nonuniform surface charge produces distortions in the equilibrium electrostatic field. The characteristic symptom of field distortion is the generation of flow velocities in all three coordinate directions, including a circulation pattern perpendicular to the main flow axis therefore severely distorting the Poisson-Boltzmann double layer. The result is an exceptionally high microbes and ions removal efficiencies from aqueous suspension by the alumina's surfaces with combined microscale and nanoscale structures that strongly suggests existence of a coupling effect of the local electrical double layer (EDL) field with the local flow field.

Keywords: point of zero charge (PZC); isoelectric point (IEP); zeta potential; electrical double layer (EDL); electrokinetic phenomena (EKP)

Abbreviations

PZC	point of zero charge
IEP	isoelectric point
EDL	electrical double layer
DL	double layer
EKP	electrokinetic phenomena
LRV	logarithm reduction value

DI RO	deionized reverse osmosis
2D	two dimensional
DLVO	Derjaguin-Landau-Verwey-Overbeek
TEM	transmission electron microscopy
SEM	scanning electron microscopy
DE	diatomaceous earth
ID	inner diameter
DW	distilled water
RT	raoultella terrigena
B. diminuta	Brevundimonas diminuta
E. coli	Escherichia coli
rms	root-mean-square

1. Introduction

For nonconducting solids, Smoluchowski [1] derived equations that are valid for any shape of a particle or pores inside a solid, provided the (local) curvature radius, a_{particle}, largely exceeds the Debye length, $\lambda_D = \kappa^{-1}$, where k is derived from the Poisson-Boltzmann theory in the Debye-Hückel approximation [2]. For 1:1 NaCl electrolyte with bulk concentration c_{NaCl} at T = 25 °C the Debye length equals to:

$$\lambda_D \cong 0.304 / \sqrt{c_{NaCl}} \text{ (in nm)} \quad (1)$$

where c_{NaCl} is the concentration of the salt, in mol/dm^3

The simplification that the surface charge is uniformly smeared along the surface renders the governing equations one-dimensional and, thereby, greatly facilitates their solution. The classical Smoluchowski equation was derived under two important approximations [1]: (*i*) the diffuse layer is rather thin as compare to the capillary radius, $a_{\text{capillary}}$, that is, $ka_{\text{capillary}} >> 1$ and (*ii*) ζ potential of the surface is low, that is, the electrical energy is small as compared to thermal energy $|\zeta ze| < k_B T$, where z is the valence of ions (assuming symmetric electrolyte, that is, $z_+ = z_- = z$), e is the electron charge, k_B is the Boltzmann constant, and T is absolute temperature. For ambient temperature of 25 °C in water it translates to $|\zeta| < 25.7$ mV for the 1:1 electrolyte. Theoretical treatments are available for calculation of streaming current in the case of cylindrical capillary [3] and for the case of a close packing of spheres [4,5].

Borghi et al. [6] observed a remarkable reduction by several pH units of the isoelectric point (IEP) on rough nanostructured surfaces, with respect to flat crystalline rutile TiO_2. In order to explain the observed behavior of IEP, Borghi et al. [6] considered the roughness-induced self-overlap of the electrical double layers as a potential source of deviation from the trend expected for flat surfaces. We recently reported an increase by about three pH units in the values of point of zero charge (PZC) of AlOOH-coated siliceous particles seen in Figure 1 with nanoscale roughness [7] as compare to smooth [8] and AlOOH-coated silica surfaces with (unspecified) nanoscale roughness [9].

Numerical models for pressure driven flow with an arbitrary but periodic patch-wise heterogeneous surface pattern over a flat heterogeneous region perpendicular to the flow axis have been developed for 2D [10,11] and for 3D [12,13,14] flows. The models were based on a simultaneous solution to the Nernst-Planck, Poisson-Boltzmann, and Navier-Stokes equations to determine the local ionic concentration, velocity vectors and electrostatic potential contours in the double layer distribution. The presence of a heterogeneous patch is shown to induce flow in all three coordinate directions, including a circulation pattern perpendicular to the main flow axis [10–14]. The normal velocities in the 2D case [10] increase linearly with pressure drop and increase with the square of the difference in magnitude between the surface charge densities of two distinctly charged patches. These velocities vary with the fifth power of the Debye length, i.e., λ^5 [10]. The difference in magnitude between the charge densities, $|\sigma_1|$ and $|\sigma_2|$, generates the normal velocities in 2D case and the subsequent electric field distortion. However, more important than just the values of $|\sigma_1|$ and $|\sigma_2|$, is the difference in their magnitudes, $\Delta\sigma$, defined as

$$\Delta\sigma = ||\sigma_1| - |\sigma_2|| \tag{2}$$

Colloid stability is often predicted by the Derjaguin-Landau-Verwey-Overbeek (DLVO) theory [15,16], which was developed for smooth, homogeneous particles with ideal geometries and with no DL overlap. Despite the success of DLVO theory, numerous investigators have modified the DLVO theory to include factors not accounted for in the DLVO model since the real colloidal systems generally contain some degree of nonuniformity, in the form of surface roughness and/or chemical heterogeneities [17–22]. The general impact of roughness is to amplify the long range behavior of noncontact DLVO forces with the approximate amplification factor of exponential force between a rough and smooth surfaces of $\exp(\sigma_{roughness}^2/\lambda_{Debye}^2)$, where $\sigma_{roughness}$ is the mean roughness [20]. Significant work has been focused on extending the precepts of the traditional DLVO model to accommodate these non-DLVO forces (energies). The effect of hemispherical asperities on the long range van der Waals and electrostatic interactions between a rough surface and smooth colloidal particle can further contribute to the distortion [19]. A review paper [22] discussed many of the interactions that play a role in environmental systems and are not commonly included in the traditional DLVO model: e.g., hydrogen bonding and the hydrophobic effect, hydration pressure, non-charge transfer Lewis acid base interactions, and steric interactions.

The purpose of this paper is to investigate the effect of nanoscale surface roughness on filtration of micron and sub-micron particles from aqueous solution by AlOOH-coated siliceous particles associated with pressure-driven flow through micrometer size pores of non-woven filter media and aluminized diatomaceous earth (DE) particles packed into a short column.

Experimental data suggest that the generation of flow velocities in all three coordinate directions, including a circulation pattern perpendicular to the main flow axis results in exceptionally high microbes and ions removal efficiencies from aqueous suspension by the alumina's surfaces with combined microscale and nanoscale structures.

2. Materials and Methods

2.1. Transmission and Scanning Electron Microscopy (TEM and SEM) Analyses

The TEM images were recorded on the JEOL JEM2010 TEM at 200 kV accelerating voltage. No coating was applied. The SEM images were recorded on the JEOL JSM6335F SEM at 5 kV.

Sample preparation for a nonconductive materials seen in Figure 1 was by applying a gold-palladium alloy by sputtering in vacuum to a thickness of a few nanometers (<5 nm). A coating of this thickness would not be visible in images at this magnification. Figure 1a and 1b shows a TEM and SEM images of the alumina nanofibers, 2 nm in diameter and approximately 0.25 μm long that are electroadhesively grafted to a microglass fiber at 40 weight percent (wt%) AlOOH loadings bonded to a 0.6 μm diameter glass microfiber. The alumina nanofibers appear as a fuzzy layer on the microglass core. The active component has been classified as quantum wire [7].

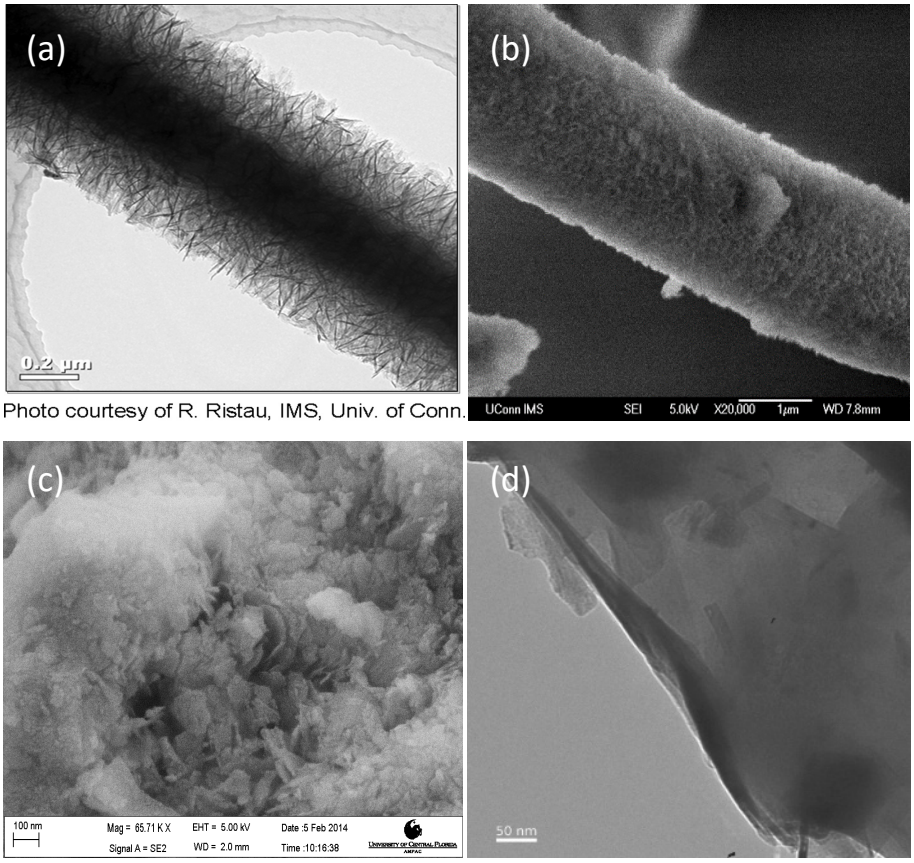

Photo courtesy of R. Ristau, IMS, Univ. of Conn.

Figure 1. TEM and SEM images of AlOOH nanostructures: (a) TEM image of boehmite nanofibers bonded to 0.6 μm diameter glass microfiber classified as "quantum wire" (see Ref. [7]); (b) SEM shows a carpet of boehmite nanofibers completely covering the glass microshaft (Courtesy Dr. R. Ristau of IMS, University of Connecticut); (c) SEM of aluminized DE60 particles; (d) TEM of aluminized DE80 particles classified as "quantum dots" (see Eqs. (13)–(17) of Ref. [7]). "Quantum dot" is a 10 × 10 × 1 boehmite cluster 1.2 nm high and 3–4 nm diameter (Courtesy Dr. A. Slesarev of Rice University).

The active component in the filter media of Ref. [7] is a nanolayer in the form of monocrystalline oxide/hydroxide (γ-AlOOH) with a thickness of approximately 1.2 nm electroadhesively deposited onto siliceous support material, thereby forming a highly positive composite. The active component has been classified as quantum dots rather than 2D continuous nanocoating [7].

2.2. Mulch Preparation

For the purpose of this study the alumina nanofiber content bonded to 0.6 μm glass microfiber scaffolding seen in Figure 1a and 1b were optimized on 20, 40 and 60 wt% of alumina loadings following a procedure described in Example 4 of Ref. [23]. No other fibers or binders were added to the mulch.

2.3. Non-woven Positive Filter Media

The filter media is manufactured and sold as non-woven media by Ahlstrom Filtration LLC under the tradename Disruptor™. Argonide Corporation manufactures the filter cartridges from Disruptor media. Polymeric fibers, primarily polyester are added for formability and pleatability. The alumina nanofibers completely occupy the available surface of the 0.6 μm glass microfiber scaffolding. The pore size of the media can be varied from about 1 to 30 μm, although a 1.0 ± 0.3 μm pore size was selected for purifying drinking water from sub-micron particles (see Table 1 below) and a 4 ± 2 μm pore size was selected as a low pressure drop prefilter to the drinking water filter element (see Table 1 below). The filter media's thicknesses are about 0.8 mm and 1.2 mm thick for drinking water filter and prefilter respectively, resulting in approximately 800 and 300 pores correspondently that a particle must transit before exiting as filtrate. The media have a rapid dynamic response for adsorbing bacteria, virus and nucleic acids from biological solutions. Typically 5 LRV (logarithm reduction value (Eq. (3)) of bacteria and 4 LRV of viruses are retained by a pleated layer at flow velocity 0.7 mm/s at a ΔP of 2–6 kPa for prefilter and 15 kPa for drinking water filter media where:

$$\mathrm{LRV} = -\log_{10}(C_{final}/C_{initial}) \tag{3}$$

where $C_{initial}$ and C_{final} are the initial and final concentrations of particles.

Table 1. Flow characteristics of nano alumina non-woven and aluminized DE filter media.

Media	Grade	Thickness (mm)	Mean particle size [a] (μm)	Bubble point (kPa)	Mean flow pore diameter, $d_{\text{mean flow}}$ (μm)	Largest pore diameter, d_{largest} (μm)
Non-woven [a]	Prefilter media [c]	1.2	~1 [a]	9.8 ± 0.8 [e]	2.3 ± 0.3	29 ± 2 [e]
	Drinking water filter media [d]	0.8	~1 [a]	20 ± 2 [e]	0.7 ± 0.3	14 ± 1 [e]
Aluminized DE [b]	Fine grade aluminized DE		10		3.0 ± 0.5	
	Medium grade aluminized DE		18		5.5 ± 1.5	
	Coarse grade aluminized DE		80		24.0 ± 3.5	

Notes: [a] Figure 1a and 1b; [b] Figure 1c and 1d; [c] Disruptor grade 5292; [d] Disruptor grade 5283; [e] Average value for 10 cartridges.

2.4. Formation of the Precoat

The precoats were formed using either a Nalgene filter holders with receiver (available from Cole-Palmer, Cat # S-06730-53) or a 25 mm diameter syringe filter holder (available from VWR, Cat # 28144-109). The precoats have surface area of ~10 cm^2 and ~3.7 cm^2, respectively, and are ~3 mm thick.

2.5. Latex Microspheres

Monodispersed polystyrene latex microspheres (beads) coated with sulfate groups with a mean diameter of 30 ± 5 nm were obtained from Duke Scientific Corporation. According to the manufacturer, the spheres have a net negative charge in aqueous solution. Particles were used as supplied by the manufacturer and re-suspended in DI RO water whose conductivity is less than 0.1 μS/cm. The charge is provided by a mixture of sulfate and hydroxyl groups on the latex surface with zeta potential of approximately $\zeta \cong -82$ mV [24].

2.6. Bacteriophages and Bacteria Preparation

Suspensions of MS2 and *fr* bacteriophages with titers of ~10^{12} particles/mL were prepared as described in Ref. [25], stored at 4 °C, and then diluted in deionized reverse osmosis (DI RO) water with conductivity less than 0.1 μS/cm. MS2 (ATCC 15597-B1) and *fr* (ATCC 15767-B1) bacteriophages are icosahedral in shape with a diameter of 26–27 nm [26] and 19 nm [27], respectively. The isoelectric point (IEP) of *fr* bacteriophage is 8.9–9.0 [27]. In this study, MS2 bacteriophage was chosen because it is often used as a surrogate for human enteric viruses and *fr* bacteriophage was chosen because it is positive in aqueous suspensions at pH range of 3–9. The zeta potential of MS2 ($\zeta \cong -(33–38)$ mV [28]).

Stocks of E. coli (ATCC 15597), Raoultella terrigena (ATCC 33257) and B. diminuta (ATCC 19146) with titers of ~10^9 particles/mL were prepared and stored at 4 °C, and then diluted in DI RO water with conductivity less than 0.1 μS/cm. E. coli bacterium has a cell IEP of 3.5 and zeta potential of $\zeta \cong -35$ mV. Zeta potential is fairly insensitive within a pH range of 6 to 9 [29]. However, it should be noted that the zeta-potential is physically meaningful only for the so-called hard colloids. Instead, the bioparticles are models of soft colloids, i.e., colloids where charges are three-dimensionally distributed [30]. For example, the IEP value of MS2 bacteriophage in different environments based on averaging of 10 measurements shows a mean IEP value of 3.5 ± 0.6 and with the discrepancy in IEP (ΔIEP) of 1.8 [31]. Two recent studies by Duek et al. [26] and Chrysikopoulos et al. [28] determined the alteration of the IEP by a change in water chemistry (e.g., ionic strength or ionic composition) with IEP of the former case in the range from less than 2 at ionic strengths of 0.0 and 2.6 mM to IEP of 4.4 in the latter case that was measured in double distilled water. Consequently, zeta-potential and IEP parameters should be interpreted very carefully for viruses with their adhesion capacity onto charged abiotic surfaces [30].

2.7. Measuring Methods

2.7.1. Streaming and Zeta Potentials

In the streaming potential process, electrolyte solution is forced through the filtration media pores by applying a pressure drop, ΔP. Because the walls of the channel are charged, the fluid adjacent to the surface bears an equal but opposite charge density, and the hydrodynamic flow carries a convection countercurrent. The net current through the cross-sectional area of the pore must be zero so that a voltage differential, $\Delta\phi$, is generated.

Zeta potential is an important and reliable indicator of the surface charge of filters. It can be deduced from experimental data, e.g., from measuring the streaming potential. It has been long recognized [32,33,34] that in the plug flow and in the networks of fibrous materials situations, the apparent zeta potential ($\zeta_{apparent}$) is a function of bulk conductivity of filtered liquid (K^L) while the true zeta potential (ζ_{true}) is a function of bulk conductivity of filtered liquid (K^L) as well as surface conductance (K^σ). The true zeta potential and specific surface conductance can be evaluated by plotting of reciprocal of the apparent zeta potential as a function of the resistivity of water. The apparent zeta potential ($\zeta_{apparent}$) was calculated using the weighted least-squared procedure [35] for at least three different conductivities of water adjusted with NaCl

$$E_{\text{streaming}} = \frac{\varepsilon_0 \varepsilon \zeta_{\text{apparent}} \Delta p}{\mu K^{\text{L}}} \tag{4}$$

where μ is the dynamic viscosity of the electrolyte solution (for water at 25 °C is equals to ~890.02 μPa·s [36]) and Δp is the differential pressure across a packed bed or non-woven media.

The true zeta potential (ζ_{true}) has contributions from both, the surface (K^σ) and bulk (K^L) conductions (see equation 4.3.41 of Ref. [37]):

$$E_{\text{streaming}} = \frac{\varepsilon_0 \varepsilon \zeta_{\text{true}} \Delta p}{\mu (K^{\text{L}} + 2K^{\sigma} / a_{\text{surface}})} \tag{5}$$

After re-arraignment we obtain:

$$1/\zeta_{apparent} = 1/\zeta_{true} + 2K^{\sigma}/\zeta_{true} a_{surface} R \tag{6}$$

where R is the resistivity of the water (in Ω·m) being filtered (by definition $R = 1/K^L$). Another way to determine the true zeta potential would be to perform additional electrical resistance measurements at high ionic strength [38].

The streaming potential is measured by means of a pair of Ag/AgCl electrodes located on both sides of two parts of a channel (ID = 19 mm) separated by a septum (three layers of two dimensional filter media having an irregular pore pattern and an irregular pore size of 0.1–0.2 mm. The aluminized DE powder was packed inside the tube on the septum with depth of 3.5–4.0 cm). A solution of a known conductivity, as measured by Oakton ECTestr Pure, is placed in a pressurized, aluminized DE-packed column and pressure in the range from 7 to 70 kPa is applied to the vessel and therefore the pressure is transferred to the filter media. The streaming potential is found by

applying at a given time an over-pressure (ΔP, bar) to the vessel and measuring the resulting potential difference ($\Delta\phi \equiv E_{streaming}$, V) on both sides of the filter bed. The $E_{streaming}$ and ΔP values are measured at ±0.1 mV and ±700 Pa, respectively. The bulk conductivity of the solutions ranged from 2.9 μS/cm for 0.03 mmol/dm^3 NaCl to 12.96 mS/cm for 0.12 mol/dm^3 NaCl solutions in deionized reverse osmosis (DI RO) water with initial conductivity less than 0.1 μS/cm. The pH values were adjusted with 1 mol/dm^3 NaOH or with 1 mol/dm^3 HCl.

2.7.2. Bubble Point of Non-woven Media

A thoroughly wetted and capped from both ends filter cartridge is immersed into a tank filled with water and air is exerted into the capped cavity. The upstream air pressure is then slowly increased, eventually resulting in the selective intrusion of air through the largest pores and formation of an air bubbles stream [39]. The pressure is recorded at the point where the first stream of bubbles is seen in the effluent. The bubble point values were determined for both, the prefilter and drinking water filter cartridges (available from Argonide Corporation, USA) used in present work. The largest pore diameter, $d_{largest}$, was determined assuming that the surface tension of the water within the media at T = 25 ^{o}C is γ = 71.97 mN/m [36] and boehmite surface is hydrophilic with the contact angle $\theta = 0^o$.

$$d_{largest} = 4\gamma\cos\theta/\Delta P_{bubble\ point} \tag{7}$$

2.8. Mean Flow Pore Diameter of Alumina's Non-woven and Aluminized DE Media

The mean flow pore diameter, $d_{\text{mean flow}}$, was determined as described in Ref. [40,41]:

$$d_{mean\ \ flow} = \sqrt{32B} / \varepsilon \tag{8}$$

where permeability $B = v\mu z/\Delta P$; v is the flow velocity through the media; μ is the viscosity; z is the thickness of the media; ΔP is the pressure drop across the media, and ε is the porosity.

Table 1 shows values of the mean flow and largest flow pore diameter of the prefilter and drinking water cartridges as well as the mean flow pore diameter of aluminized DE powders packed in empty refillable canisters (available from Watts Filtration, Cat # RC-C-975).

3. Results and Discussion

3.1. Non-woven Media

The filter's active component is a nanoalumina fiber with an external surface area of ~500 m^2/g (see Figure 1a and 1b). It has been identified as crystalline boehmite (AlOOH) using x-ray diffraction [7]. Boehmite nanofibers create high zeta potential ($\zeta_{true} \geq 46$ mV) in aqueous solutions in the pH range of 3–8. The point of zero charge (PZC) of alumina non-woven media was determined to be 11.6 ± 0.2 [7].

3.1.1. Sorption Capacity Measurements Using Latex Spheres

Figure 2 shows breakthrough curves of 30 nm size latex spheres (beads) by a 0.8 mm thick layer of nanoalumina filter of at a flow velocity of 0.17 mm/s. The sorption capacity is approximately proportional to the nanoalumina fiber loading.

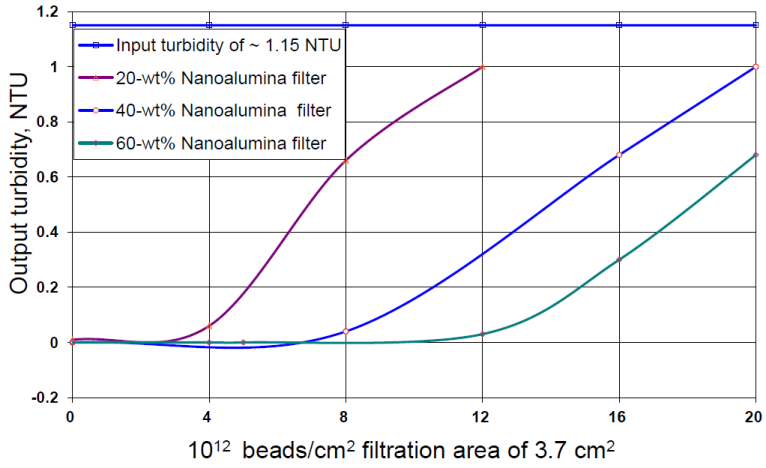

Figure 2. Breakthrough curves of 30 nm latex spheres at input concentration of 10^{12} particle/mL through 3.7 cm^2 surface area as a function of AlOOH content.

3.1.2. Correlation of Zeta Potential and Initial Removal Efficiency of Biological Particles

Table 2 shows correlation of zeta potential with bacteriophages, and bacteria removal efficiencies by one and two layer of 35 wt% nanoalumina/microglass media at flow velocity of 0.7 mm/s.

Table 2. Correlation of zeta potential with initial removal efficiency of bioparticles by alumina nanofiber media as a function of pH.

pH	ζ potential (mV)	*fr* removal efficiency, LRV [b]		MS2 removal efficiency, LRV [b]	PRD-1 removal efficiency, LRV [b]	E. coli removal efficiency, LRV [b]	B. diminuta removal efficiency, LRV [b]
		1 layer [c]	2 layers [c]	2 layers [c]	2 layers [c]	2 layers [c]	2 layers [c]
3	46 ± 7 [a]	3.0 ± 0.3	5.0 ± 0.3				
5	46 ± 7 [a]	>6.2	>6.2	>5.0			
7	47 ± 9 [a]	>6.2	>6.2	>6.0	>7.0	>7.5	>7.6
8	46 ± 6 [a]	>6.1	>6.1	>5.0		6.3	>6.2
9	26 ± 4 [a]	>6.0	>6.0	>5.0			
10	23 ± 5 [a]	4.2 ± 0.3	>6.0				
11	22 ± 5 [a]	0.2 ± 0.2	1.5 ± 0.7				

Notes: [a] Ref. [7]; [b] Logarithm reduction value; [c] By 1- or 2-layers of drinking water filter media (Table 1) at flow velocity of 0.7 mm/s.

Initial removal efficiencies are high for both bacteriophages and bacteria. Most bacteria and most other contaminants encountered in nature are negatively charged in water with notable exception of the *fr* bacteriophage that is positive at pH less than about 8.9–9.0 [27]. Yet, the initial removal efficiency for the *fr* bacteriophage at pH = 7 is high as well (see Table 2), i.e., >99.9999% with a double layer of the media at a flow velocity 0.7 mm/s.

3.1.3. Removal Efficiency of Biological Particle at Different Salinities

Table 3 shows removal efficiencies of MS2 bacteriophage and RT bacteria at neutral pH = 7 by a single layer of non-woven prefilter media in a form of pleated cartridge with surface area of 0.3 m^2 as a function of flow velocity and electrolyte ionic strength.

Table 3. Microbial removal efficiencies by non-woven prefilter pleated cartridge.

Electrolyte ionic strength, NaCl (mM)	λ_D [a] (nm)	Flow velocity (mm/s)	Contact time (s)	Brownian displacemen [b] of RT (μm)	Brownian displacemen [b] of MS2 (μm)	MS2 removal efficiency, LRV [c]	RT removal efficiency, LRV [c]
0.002(1) [d]	215	0.05	22.5	4.7	28	>6.4	6.4 ± 0.7
		0.2	5.6	2.4	14	>6.4	6.2 ± 1.0
		0.8	1.4	1.2	7.0	>6.4	5.8 ± 0.4
		3.4	0.35	0.6	3.5	>6.4	6.0 ± 0.5
0.05(1) [d]	43	0.05	22.5	4.7	28	>5.7	5.9 ± 0.2
		0.2	5.6	2.4	14	>5.7	5.8 ± 0.2
		0.8	1.4	1.2	7.0	>5.7	5.6 ± 0.2
		3.4	0.35	0.6	3.5	>5.7	5.2 ± 0.6
0.35(4) [d]	16	0.05	22.5	4.7	28	>5.2	5.8 ± 0.2
		0.2	5.6	2.4	14	>5.2	5.3 ± 0.2
		0.8	1.4	1.2	7.0	>5.2	5.2 ± 0.4
		3.4	0.35	0.6	3.5	>5.2	5.0 ± 0.8
1.0(1) [d]	9.6	0.05	22.5	4.7	28	>6.6	5.7 ± 0.4
		0.2	5.6	2.4	14	>6.6	5.2 ± 0.5
		0.8	1.4	1.2	7.0	5.6 ± 0.2	4.8 ± 0.5
		3.4	0.35	0.6	3.5	5.1 ± 0.2	4.4 ± 0.5
3.0(3) [d]	5.5	0.05	22.5	4.7	28	>5.8	4.9 ± 0.3
		0.2	5.6	2.4	14	>5.8	4.6 ± 0.3
		0.8	1.4	1.2	7.0	>5.8	4.2 ± 0.7
		3.4	0.35	0.6	3.5	5.2 ± 0.6	4.3 ± 0.9
10(1) [d]	3.0	0.05	22.5	4.7	28	>5.9	4.2 ± 0.2
		0.2	5.6	2.4	14	>5.9	4.1 ± 0.2
		0.8	1.4	1.2	7.0	>5.9	3.7 ± 0.3
		3.4	0.35	0.6	3.5	4.7 ± 0.3	3.7 ± 0.4
40(4) [d]	1.5	0.05	22.5	4.7	28	4.8 ± 0.2	3.9 ± 0.2

		0.2	5.6	2.4	14	5.1 ± 0.3	3.7 ± 0.4
		0.8	1.4	1.2	7.0	4.7 ± 0.2	3.1 ± 0.4
		3.4	0.35	0.6	3.5	3.1 ± 0.2	2.8 ± 0.5
100(10) [d]	0.96	0.05	22.5	4.7	28	>4.5	4.0 ± 0.5
		0.2	5.6	2.4	14	>4.5	3.7 ± 0.4
		0.8	1.4	1.2	7.0	>4.5	3.1 ± 0.4
		3.4	0.35	0.6	3.5	3.5 ± 0.3	2.8 ± 0.4
250(25) [d]	0.61	0.05	22.5	4.7	28	4.2 ± 1.0	3.1 ± 0.2
		0.2	5.6	2.4	14	3.7 ± 0.3	2.7 ± 0.2
		0.8	1.4	1.2	7.0	3.0 ± 0.2	2.5 ± 0.2
		3.4	0.35	0.6	3.5	1.2 ± 0.2	1.8 ± 0.2
510(51) [d]	0.43	0.05	22.5	4.7	28	2.3 ± 0.6	2.4 ± 0.6
		0.2	5.6	2.4	14	1.8 ± 0.2	2.2 ± 0.4
		0.8	1.4	1.2	7.0	1.8 ± 0.4	1.9 ± 0.2
		3.4	0.35	0.6	3.5	1.0 ± 0.5	1.5 ± 0.4
3000(300) [d]	0.18	0.05	22.5	4.7	28	2.1 ± 0.3	2.0 ± 0.3
		0.2	5.6	2.4	14	1.6 ± 0.3	1.6 ± 0.2
		0.8	1.4	1.2	7.0	1.3 ± 0.3	1.4 ± 0.2
		3.4	0.35	0.6	3.5	1.3 ± 0.5	1.0 ± 0.2

Notes: [a] Calculated with the use of equation (1); [b] Calculated with the use of equation (9); [c] Logarithm reduction value; [d] Error limits in parentheses are accuracy in the units of the last digit reported.

The electrolyte ionic strength was adjusted with NaCl salt (purity > 99.0%) that was added to distilled water (DW) with conductivity less than 0.1 μS/cm. An aliquot of 15–20 mL of MS2 suspension was added whose input concentration was ~5.0×10^9 particles/mL with a conductivity of ~28 μS/cm together with an aliquot of 12 mL of washed in DW water RT bacteria whose input concentration was ~5.0×10^9 particles/mL to 50 L of the DW water. After passing 5 liters of the suspension at a specified flow rate, a 250 mL aliquot was collected. The sample was serially diluted by a factor of 10 and analyzed as plaque forming units (PFU) for counting MS2 bacteriophages with the use of the double-layer method [25,42]. Briefly, dilutions of each sample were mixed with host cells, plated on nutrient agar, and incubated overnight. The resulting plaque counts were converted to PFU/mL. The RT bacteria was enumerated with the use of a membrane method [43] for counting coliform forming units (CFU).

Results of Table 3 indicate that the MS2 and RT removal efficiencies do not depend within 2σ accuracy on the flow velocity in the range from 0.05 to 3.4 mm/s and at contact times from 0.35 to 22.5 seconds for electrolyte's ionic strength less than 1 mmol. Application of the Stokes-Einstein equation [44]:

$$\left\langle x \right\rangle_{Brownian}^2 / 2t = k_B T / 6\pi\mu a \tag{9}$$

to a spherical particle suspended in water (μ = 890.02 μPa·s at 25 °C [36]) produces a root-mean-square (rms) displacements for MS2 virus and RT bacteria (see Table 3) that are much lesser than the

radius of the largest pore of $a_{largest}$ = 15 ± 1 μm (see Table 1). Yet, the removal efficiencies at ionic strengths less or equal to 0.35 m*M* is greater than 99.999%.

Such a behavior can be described based on the characteristic effect of the local EDL field distortion by generating of circulating velocity pattern normal to the flow direction.

3.2. Aluminized Diatomaceous Earth (DE)

Aluminum oxide-hydroxide nanolayer (AlOOH) with estimated thickness of 1.2 nm (see Eqs. (13)–(17) of Ref. [7]) was deposited onto siliceous DE support material as described in Ref. [45]. Figure 3 indicates that aluminized DE18 powders with average particle size of 18 μm are highly positive (ζ > +50 mV) at aluminum oxide/hydroxide solids loading greater than ~20 wt% as compared to the highly negative character of the bare DE18 support (ζ ~ −70 mV). Alumina's nanolayer surface can be further functionalized by adding other sub-micron or nano-size particles to target a specific contaminant. For example, aluminized DE coated with nano-size iron monohydrate (FeOOH) yields an arsenic sorbent that shows high sorption capacity (see Examples 15 and 16 of Ref. [45]).

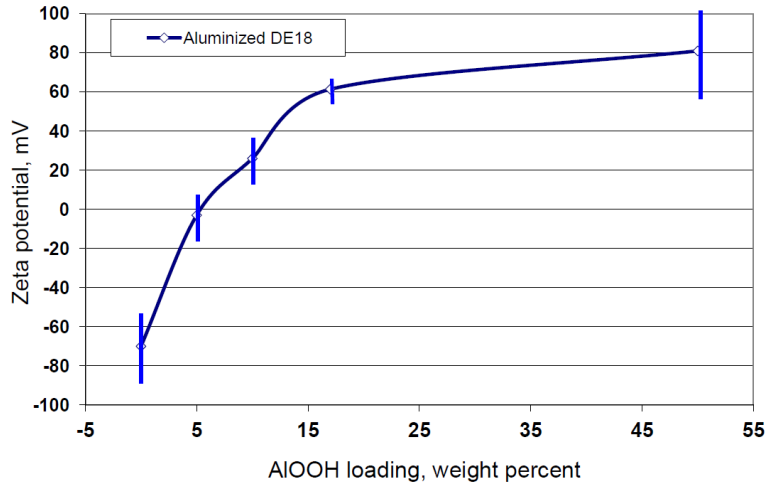

Figure 3. Zeta potential of DE18/aluminized DE18 as a function of AlOOH loading at pH = 7.

3.2.1. Adsorbtion of Soluble ^{59}Co Isotope in Short Packed Column

Similar behavior to that described in Section 3.1.3 was observed while adsorbing soluble ^{59}Co isotope in short packed columns of aluminized DE60 (see Table 4) with average particle size of 48 μm and mean flow pore size of $d_{mean\ flow}$ = 14.5 ± 2.5 μm (see Table 1) where the adsorption efficiency does not depend on flow velocity in the range from 3.3 to 10 mm/s and at contact times from 5 to 60 seconds. Similarly to the microbial removal efficiencies such a behavior can be described based on the characteristic effect of local EDL field distortion by generating of circulating velocity pattern normal to the flow direction.

Table 4. Cobalt removal efficiencies by aluminized DE60 powders packed in short columns.

Bed volume (dm^3)	pH	Column depth (mm)	Flow velocity (mm/s)	Contact time (s)	Input ^{59}Co concentration (ppb)	Output ^{59}Co concentration (ppb)	Removal efficiency (%)
0.16	10	50	10	5.0	635	<5	>99.2
0.32	10	100	6	17	635	<5	>99.2
0.64	10	200	3.3	60	635	<5	>99.2
0.16	8	50	10	5.0	656	<5	>99.2
0.32	8	100	6	17	656	<5	>99.2
0.64	8	200	3.3	60	656	<5	>99.2

3.2.2. Generation of Velocities Normal to the Surface: a 2D Case

The incorporation of a nonuniform surface charge in the streaming potential process beyond the one-dimensional analysis and by not restricting the solution to low charges was first undertaken in Refs. [10,11]. Particularly, it was shown how the nonuniform surface charge will affect the value of the zeta potential by over 30% higher than expected value due to a severe distortion of Poisson-Boltzmann EDL field especially at the ionic strengths less than 1 m*M*. Numerical model as well as a first order perturbation theory model for pressure driven flow through a slit with an arbitrary but periodic patchwise heterogeneous surface pattern has been developed for a 2D case [10,11]. The impact of bipolar surface charge distributions on pressure-driven transport has been investigated theoretically in Ref. [46] for systems with weakly charged nanopores with radius smaller than the Debye screening length.

3.2.3. Biological Particle Removal Efficiency by a Mixture of Opposively Charged Particles

The surfaces of DE80 and aluminized DE80 have similar but opposite values of ζ potentials. In such a case, there is an excess of positive ions over the DE surface but negative ions dominate over the aluminized DE surface to balance out the positive surface charge. The difference in the surface potential results in an electrostatic potential gradient within the double layer region near the transition zone between the two regions. The presence of this potential gradient results in a body force on the microbes and/or ions in the double layer; however, in this case an opposite body force is applied to the negative ions over the positively charged particle. As a result, the net body force over the region is zero and the circulation velocity perpendicular to the main flow becomes negligible. Table 5 provides experimental evidence of such behavior when mixing together the DE80 and aluminized DE80 powders, the resulting mix formed in a 3 mm precoat is losing properties of the aluminized DE tested in the same configuration. This is consistent with the case when one of the neighboring particles has opposite sign of the surface charge, i.e., $-|\sigma_2|$ for DE, than other neighboring particles, i.e., $+|\sigma_1|$ for aluminized DE (see Eq. (2)).

Furthermore, Table 5 provides an estimate of number of layers formed by aluminized DE particles arranged a group of four neighboring particles in the plane perpendicular to the flow in a 3 mm thick precoat as a function of weight percent of DE in the aluminized DE/DE mix. The

estimate shows some correlation between a number of layers formed by four neighboring aluminized DE particles and the LRV values (see Eq. (3)) of MS2 virus and RT bacteria.

Table 5. Removal efficiency of MS2 viruses and RT bacteria in a 3 mm thick precoat by a mix of DE80 and aluminized DE80 powders.

Percent of DE in aluminized DE/DE precoat	Number of layers formed by aluminized DE [c]	MS2 removal efficiency [a], LRV [b]	RT removal efficiency [a], LRV [b]
0	40	6.1 ± 0.1	>7.7
10	38	5.1 ± 0.2	>7.7
25	16	3.6 ± 0.4	3.9 ± 0.3
50	7	2.6 ± 0.9	3.0 ± 0.3
75	2	1.0 ± 0.2	2.2 ± 0.1
100	0	0.5 ± 0.1	0.7 ± 0.2

Notes: [a] At flow velocity of 0.67 mm/s; [b] Logarithm reduction value; [c] Arranged in a group of four neighboring aluminized DE particles in the plane perpendicular to the flow.

3.2. Surface Conductance and Zeta Potential of Aluminized DE Powder and Non-woven Filter Media

Figure 4 compares values of true zeta potential, ζ_{true}, and surface conductance, K^{σ}, of aluminized DE powder as well as non-woven drinking water filter media. In both cases, the K^{σ} values are greater by two order of magnitude at pH3 and pH12 as compare to the values at neutral pH in the range from pH = 6 to pH = 8. In addition, the K^{σ} values of aluminized DE are greater than these of non-woven filter media by a factor of 4.6 ± 3.0 over the pH range of 3–12.

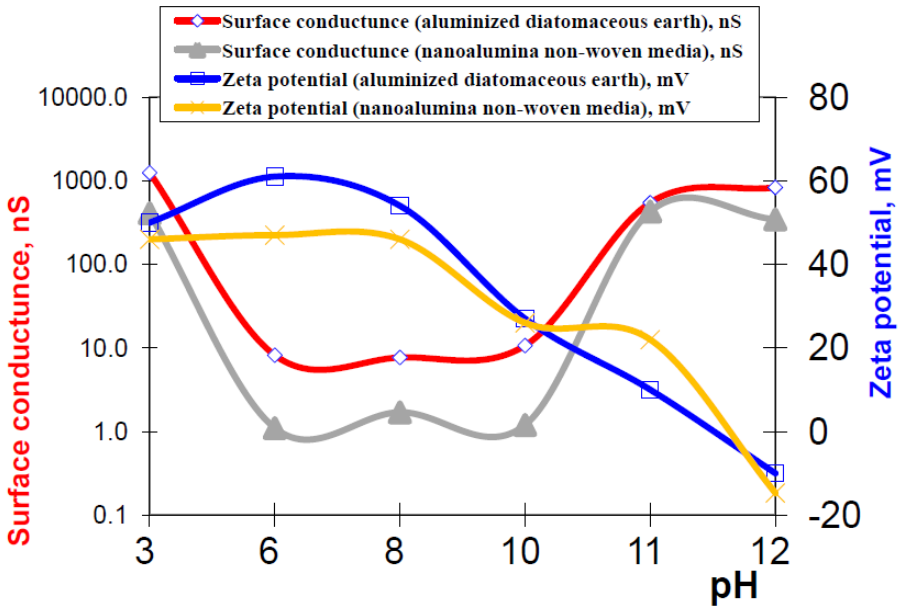

Figure 4. Surface conductance and zeta potential of aluminized DE powder and non-woven drinking water filter media.

4. Conclusion

This paper demonstrates how the positive charge properties of alumina's surfaces with combined microscale and nanoscale structures dispersed in aqueous solution can be used as a means of collecting submicron and micron particles such as viruses, bacteriophages, and bacteria. Because the nonuniformity in charge in the direction of the applied pressure drop, circulation velocities are generated that represents a symptom of electric field distortion. The larger the electric field distortion, the greater the deviation is for the zeta potential from its expected value for a smooth surface at a given pH. Experimental data suggest that the circulation velocities increase with applied pressure drop.

The most remarkable result of our studies is the observation of the shift of the point of zero charge (PZC) of quantum dot (aluminized DE, Figure 1c and 1d) and quantum wire (Figure 1a) assembled nanostructures in the form of monocrystalline oxide/hydroxide by more than three pH units towards more basic character with respect to reference γ-AlOOH crystalline surfaces.

Acknowledgements

We thank Dr. R. Ristau of IMS, University of Connecticut for providing us with TEM and SEM images of alumina nanofibers bonded to glass and microfibers (Figures 1a and 1b) and Dr. A. Slesarev of Rice University for providing us with SEM, and TEM images of aluminized DE powders (Figures 1c and 1d).

Conflict of Interest

No potential conflict of interest was reported by the authors.

References

1. Von Smoluchowski M (1921) *Handbuch der Electrizität und des Magnetismus*, 2: 366–428.
2. Lyklema J (1991) *Fundamentals of Interface and Colloid Science: Fundamentals*, London: Academic Press.
3. Rice CL, Whitehead P (1965) Electrokinetic flow in a narrow cylindrical capillary. *J Phys Chem* 69: 4017–4024.
4. O'Brien RW, Perrins WT (1984) The electrical conductivity of a porous plug. *J Colloid Interf Sci* 99: 20–31.
5. Dukhin AS, Shilov V, Borkovskaya Y (1999) Dynamic electrophoretic mobility in concentrated dispersed systems. Cell model. *Langmuir* 15: 3452–3457.
6. Borghi F, Vyas V, Podesta A, et al. (2013) Nanoscale roughness and morphology affect the isoelectric point of titania surfaces. *PLoS One* 8: e68655.
7. Kaledin LA, Tepper F, Kaledin TG (2016) Pristine point of zero charge (p.p.z.c.) and zeta potentials of boehmite's nanolayer and nanofiber surfaces. *Int J Smart Nano Mater* 7: 1–21.
8. Ermakova L, Bogdanova N, Sidorova M, et al. (2010) Electrosurface characteristics of oxide nanolayers and nanopore membranes in electrolye solutions. In: Starov VM, *Nanoscience: Colloidal and Interfacial Aspects*, Boca Raton: CRC Press, Taylor & Francis group, 193–220.

9. Rezwan K, Meier LP, Gauckler LJ (2005) Lysozyme and bovine serum albumin adsorption on uncoated silica and AlOOH-coated silica particles: the influence of positively and negatively charged oxide surface coatings. *Biomaterials* 26: 4351–4357.
10. Cohen RR, Radke CJ (1991) Streaming potentials of nonuniformly charged surfaces. *J Colloid Interf Sci* 141: 338–347.
11. Cohen RR (1987) Equilibrium and dynamic properties of the charged aqueous/clay interface [PhD thesis]. University of California.
12. Li D (2004) *Electrokinetics in microfluidics*, Amsterdam: Elsevier.
13. Erickson D, Li D (2002) Microchannel flow with patchwise and periodic surface heterogeneity. *Langmuir* 18: 8949–8959.
14. Erickson D, Li D (2001) Streaming potential and streaming current methods for characterizing heterogeneous solid surfaces. *J Colloid Interf Sci* 237: 283–289.
15. Derjaguin BV, Landau L (1941) Theory of stability of strongly charged lyophobic sols of the adhesion of strongly charge particles in solution electrolytes (in russian). *Acta Physicochim USSR* 14: 633–662.
16. Verwey EJ, Overbeek JTG (1948) *Theory of the Stability of Lyophobic Colloids*, Amsterdam: Elsevier.
17. Hoek EMV, Agarwal GK (2006) Extended DLVO interactions between spherical particles and rough surfaces. *J Colloid Interf Sci* 298: 50–58
18. Duval JFL, Leermakers FAM, van Leeuwen HP (2004) Electrostatic interactions between double layers: influence of surface roughness, regulation, and chemical heterogeneities. *Langmuir* 20: 5052–5065.
19. Walz JY, Suresh L, Piech M (1999) The effect of nanoscale roughness on long range interaction forces. *J Nanopart Res* 1: 99–113.
20. Parsons DF, Walsh RB, Craig VSJ (2014) Surface forces: Surface roughness in theory and experiment. *J Chem Phys* 140: 164701.
21. Henry C, Minier JP, Lefèvre G, et al. (2011) Numerical Study on the Deposition Rate of Hematite Particle on Polypropylene Walls: Role of Surface Roughness. *Langmuir* 27: 4603–4612.
22. Grasso D, Subramaniam K, Butkus M, et al. (2002) A review of non-DLVO interactions in environmental colloidal systems. *Rev Environ Sci Biotechnol* 1: 17–38.
23. Tepper F, Kaledin L (2005) Nanosize electropositive fibrous adsorbent. US patent 6,838,005.
24. Velev OD, Furusawa K, Nagayama N (1996) Assembly of latex particles by using emulsion droplets as templates. 1. Microstructured hollow spheres. *Langmuir* 12: 2374–2384.
25. International Organization for Standardization (1995) ISO 10705-1 Water quality—Detection and enumeration of bacteriophages—Part 1. Enumeration of F-specific RNA bacteriophages, Geneve, Switzerland.
26. Duek A, Arkhangelsky E, Krush R, et al. (2012) New and Conventional Pore Size Tests in Virus-Removing Membranes. *Water Res* 46: 2505–2514.
27. Herath G, Yamamoto K, Urase T (1999) Removal of Viruses by Microfiltration Membranes at Different Solution Environments. *Water Sci Technol* 40: 331–338.
28. Chrysikopoulos CV, Syngouna VI (2012) Attachment of Bacteriophages MS2 and ΦX174 onto Kaolinite and Montmorillonite: Extended-DLVO Interactions. *Colloid Surface B* 92: 74–83.
29. Lin DQ, Brixius PJ, Hubbuch JJ, et al. (2003) Biomass/Adsorbent Electrostatic Interactions in Expanded Bed Adsorption: A Zeta Potential Study. *Biotechnol Bioeng* 83: 149–157.

30. Dika C, Duval JF, Francius G, et al. (2015) Isoelectric point is an inadequate descriptor of MS2, Phi X 174 and PRD1 phages adhesion on abiotic surfaces. *J Colloid Interf Sci* 446: 327–334.
31. Michen B, Graule T (2010) Isoelectric Points of Viruses. *J Appl Microbiol* 109: 388–397.
32. Oulman CS, Baumann ER (1964) Streaming potentials in diatomite filtration of water. *J Am Water Works Ass* 56: 915–930.
33. Briggs DR (1928) The determination of the ζ potential on cellulose-a method. *J Phys Chem* 32: 641–675.
34. Mossman CE, Mason SG (1959) Surface electrical conductance and electrokinetic potentials in networks of fibrous materials. *Can J Chem* 37: 1153–1164.
35. Marquardt DW (1963) An algorithm for least-squares estimation of nonlinear parameters. *J Soc Ind Appl Math* 11: 431–441.
36. Haynes WM, Lide DR, Bruno TJ (2012) *CRC Handbook of Chemistry and Physics*, 93rd Edition, Boca Raton: CRC Press, Taylor and Francis Group.
37. Lyklema J (1995) *Fundamentals of Interface and Colloid Science: Solid-Liquid Interfaces*, San Diego: Academic Press.
38. Szymczyk A, Fievet P, Foissy A (2002) Electrokinetic characterization of porous plugs from streaming potential coupled with electrical resistance measurements. *J Colloid Interf Sci* 255: 323–331.
39. Johnston PR (1992) *Fluid sterilization by filtration*, Buffalo Grove: Interpharm Press.
40. Tepper F, Kaledin LA (2008) Drinking water filtration device. US patent 7,390,343.
41. Tepper F, Kaledin LA (2006) Electrostatic air filter. US patent 7,311,752
42. Pepper IL, Gerba CP (2004) *Environmental Microbiology: A Laboratory Manual*, Amsterdam: Elsevier.
43. US Environmental Protection Agency (1986) SW-846 Test Method 9132: Total coliform: Membrane-filter technique.
44. Einstein A (1956) *Investigations on the theory of the Brownian movement*, New York: Dover Publications (English translation of original publications).
45. Kaledin LA, Tepper F, Kaledin TG (2016) Aluminized Siliceous Powder and Water Purification Device Incorporating the Same. US Patent 9,309,131.
46. Szymczyk A, Zhu H, Balannec B (2010) Ion rejection properties of nanopores with bipolar fixed charge distributions. *J Phys Chem B* 114: 10143–10150.

AIMS Press